Journal of ELECTRONIC MATERIALS
DOI: 10.1007/s11664-013-2966-4
© 2014 TMS

Layered Growth of Lattice-Mismatched $Ga_xIn_{1-x}P$ on GaP Substrates by Liquid Phase Epitaxy

XIN ZHAO,[1,2] KYLE H. MONTGOMERY,[1] and JERRY M. WOODALL[1]

1.—Department of Electrical and Computer Engineering, University of California, Davis, CA 95616, USA. 2.—e-mail: xinzhao@ucdavis.edu

We report layered growth of $Ga_xIn_{1-x}P$ on GaP substrates using single-step liquid phase epitaxy (LPE) with a Sn-based melt when the lattice mismatch is greater than 0.4 % ($x < 0.95$). Compositional control was observed by (1) varying the cooling rate and (2) changing the melt-back temperature at the beginning of the growth. Possible growth mechanisms are proposed to explain the principles of both approaches of compositional control. Smooth epilayers have been observed. High resolution x-ray diffraction was used to characterize the composition of the epilayers, and room temperature photoluminescence was reported for one of the samples with the composition of $x = 0.11$. Plan-view TEM measurements revealed threading dislocation densities on the order of 10^8 cm^{-2} in the upper regions of the $Ga_xIn_{1-x}P$ epilayers. In contrast, when using In-based melts, LPE of $Ga_xIn_{1-x}P$ on GaP (100) substrates exhibited island growth at large misfits, whereas edge growth dominated when using GaP (111B) substrates under equivalent growth conditions.

Key words: GaInP, GaP, liquid phase epitaxy, photoluminescence, high resolution x-ray diffraction, layered growth

INTRODUCTION

$Ga_xIn_{1-x}P$ is a III-V semiconductor alloy of vital importance in visible wavelength optoelectronic devices. For example, $Ga_{0.5}In_{0.5}P$ lattice matched to GaAs is the material of choice for red light emitting diodes (LED). However, the current fabrication process of red LED is complicated. Typically, a thin $Ga_{0.5}In_{0.5}P$ epilayer is grown on a GaAs substrate. This structure is then wafer-bonded to a GaP carrier substrate and the GaAs substrate is subsequently removed by lapping or chemical lift-off.[1] Therefore, growing $Ga_xIn_{1-x}P$ directly on GaP with a single-step growth process will not only provide an alternative way of fabricating red LED at a lower cost but also improve the quantum efficiencies of these LED.

Furthermore, liquid phase epitaxy (LPE) is known for producing high quality Al-rich alloys.[2] High purity, Al-rich (Al,Ga,In)P epilayers are difficult to achieve by vapor-phase epitaxial techniques, such as metalorganic chemical vapor deposition (MOCVD) or molecular beam epitaxy (MBE), because of aluminum's tendency to oxidize rapidly. In using LPE, this work provides a path towards Al-rich (Al,Ga,In)P alloys that emit in the green part of the spectrum, thereby addressing the notorious "green gap".[3]

Finally, CuPt ordering is a common problem in growing $Ga_xIn_{1-x}P$ by the vapor-phase epitaxy approaches.[4] However, CuPt-B type ordering is generally not seen in crystals grown by LPE, due to its dense liquid–solid growth interface which prevents surface reconstruction during growth.[5]

Despite these motivations, few reports have discussed the growth of $Ga_xIn_{1-x}P$ on GaP substrates by LPE. In general, layered growth of $Ga_xIn_{1-x}P$ on lattice-mismatched substrates by LPE is difficult to achieve. For example, Nishizawa and Yoshida[6] showed that the growth of $Ga_xIn_{1-x}P$ on GaP substrates at large misfit using an In-based melt yields columnar growth. Alternatively, an effort to grow $Ga_xIn_{1-x}P$ lattice-mismatched on GaAs substrates by LPE using an epitaxial lateral overgrowth

(Received August 11, 2013; accepted December 20, 2013)

Published online: 10 January 2014

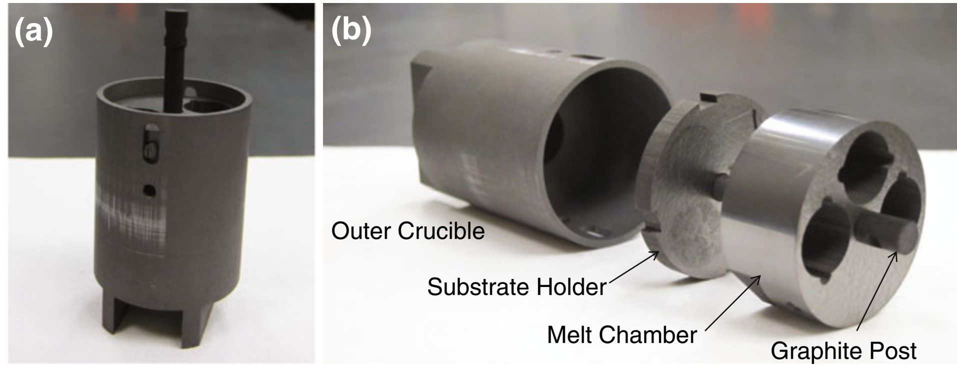

Fig. 1. (a) Assembled view and (b) exploded view of the high purity graphite apparatus used for LPE.

technique results in the growth of separate strips, which saturate at a certain width and cannot cover the entire lateral surface.[7,8]

In this work, we present a way to realize layered growth of $Ga_xIn_{1-x}P$ on GaP using a Sn-based melt by LPE. Further, we compare the surface morphology of these samples with those grown from an In-based melt.

EXPERIMENTAL PROCEDURE

For this work, a custom LPE system was utilized. The system is comprised of a vertical tube furnace, fused quartz tube, and a high-purity graphite apparatus (Fig. 1) for containing the melt and holding the substrate. The apparatus is known as the "rotating chamber," initially developed by Woodall and Hovel[9] and further customized for this work by Montgomery.[10] Since the growth procedures differed with the use of an In- and Sn-based melts, they will be discussed separately.

For the growth of $Ga_xIn_{1-x}P$ using an In-based melt, both GaP (100) and GaP (111B) substrates were used. Surface pre-treatment was performed using an $HCl:H_2O_2:H_2O$ (1:1:1) solution for 3 min to remove any residual organics and native oxide,[11] followed by a DI H_2O rinse. After the surface pre-treatment, the GaP substrates were loaded into the substrate holder and initially positioned under a covered spot of the melt chamber (Fig. 1b) to prevent phosphorous evaporation. However, it was later discovered that this also prevented the surface oxide from decomposing,[12] leading to growth on only part of the substrate, as will be shown in the "Results". Therefore, the remaining substrates were all placed under an exposed position of the melt chamber. With the substrate in place, 99.999 % pure In, 99.99999 % pure Ga, and an undoped InP polycrystalline source wafer, with a mass in excess of the solubility limit, were loaded into an open spot of the melt chamber, next to the substrate. The In:Ga weight ratio was chosen such that the expected composition, x, in the $Ga_xIn_{1-x}P$ epilayer lies within the range of 0.8–0.95 according to the ternary phase diagram.[13] The graphite parts were then loaded into the quartz tube, which was purged with high purity forming gas (4 % H_2 in N_2). The apparatus was brought to 800 °C and kept at temperature for 2 h, allowing the melt to reach equilibrium. Finally, the substrates were rotated into position under the melt and the temperature was lowered at a rate of 0.1 °C/min to commence growth. The total temperature drop was 5 °C. At the end of growth, the substrate was rotated out of the melt and the whole apparatus was cooled to room temperature prior to removal from the furnace.

For the growth of $Ga_xIn_{1-x}P$ using a Sn-based melt, the first sample was grown on a GaP (111B) substrate. After going through the same surface pre-treatment, as discussed above, the substrates were placed in an exposed position of the melt chamber. The 99.998–99.999 % pure Sn and an undoped InP polycrystalline source wafer were loaded into an open spot of the melt chamber, next to the substrate. In this case, the mass of the InP source wafer was limited to be less than the solubility limit. The graphite parts were then loaded into the quartz tube, which was purged with high purity forming gas (4 % H_2 in N_2). The apparatus was then brought to 700 °C and kept at temperature for 2 h, allowing the melt to reach equilibrium. The thickness of the melt was approximately 0.5–0.6 cm. Finally, the substrate was rotated under the melt, followed by immediate temperature change.

Since the amount of InP initially provided was insufficient to saturate the Sn melt at 700 °C,[14] the introduction of the GaP substrate into the melt would lead to etchback, as the GaP dissolved to supply P and Ga species until the solubility limit was reached. Growth took place as the apparatus was cooled for 50 °C at a rate of 0.33 °C/min. Following this cooling, the substrate remained under the melt when the furnace was turned off and cooled to room temperature. Additional samples were grown on GaP (100) substrates using a similar technique, but with varying cooling rates (0.33, 3, and 5 °C/min) and the introduction of a "melt-back" step with 0, 5, and 10 °C of melt-back whereby the furnace temperature was increased immediately prior to growth.

Nomarski micrographs were taken from an Olympus Model BHM Metallurgical Microscope with MS Plan Objectives and Nomarski DIC prisms. Scanning electron microscope (SEM) images were collected using an FEI Nova NanoSEM 430. Energy-dispersive x-ray spectroscopy (EDS) line scans were obtained from a FEI XL30 SEM with an Oxford Instruments X-Max Silicon Drift Detector (SDD). XRD analysis was performed using a Panalytical X'Pert Pro MRD equipped with a 2-bounce Ge [220] hybrid monochromator. In determining the composition from XRD data, Vegard's law was used when x was between 0.5 and 1, whereas a bowing parameter of -0.1614 was introduced when x was between 0 and 0.5 in $Ga_xIn_{1-x}P$.[15] Continuous-wave photoluminescence (cw-PL) was performed using a 552-nm diode laser with an output power of 20 mW (Coherent OBIS). Excitation and collection were performed at approximately 45° from the surface normal to the sample. The emitted signal was introduced into a spectrograph (Acton Research SP300i) and collected by a thermoelectric-cooled charge-coupled device (CCD) array detector (Andor DB-401-UV CCD). The spectrograph was calibrated using an Oriel Hg-Ne spectral calibration lamp and is accurate to ±0.5 nm. Composition determined from PL was derived assuming $E^{InP} = 1.353$ eV, $E^{GaP} = 2.777$ eV, and a bowing parameter of 0.65.[16]

RESULTS AND DISCUSSION

The surface morphology of the samples grown from an In-based melt on GaP (100) substrates is shown in Fig. 2. For the sample which stayed in the covered spot of the melt chamber during temperature ramp-up, island growth occurred on only part of the substrate as indicated by Fig. 2a. This partial growth could be attributed to the surface oxide, which was protected from decomposition by the melt chamber at elevated temperatures. The reason that the surface oxide did not dissolve in the melt is because phosphorous oxide has a more negative Gibbs free energy of formation than that of indium oxide or tin oxide at corresponding growth temperatures. Therefore, it is thermodynamically unfavorable for In or Sn to reduce phosphorous oxide into P, which can be dissolved in the melt. To resolve the problem, GaP substrates were exposed to forming gas at elevated temperatures for the oxide to decompose. However, since P has a high vapor pressure, the GaP substrates must be pre-treated with a solution containing HCl to avoid P evaporation. Our experiments showed that the GaP substrate pre-treated with HCl preserved its surface morphology after being exposed to forming gas for 3 h at 800 °C. On the contrary, GaP substrates pre-treated with NH_4OH suffered from surface

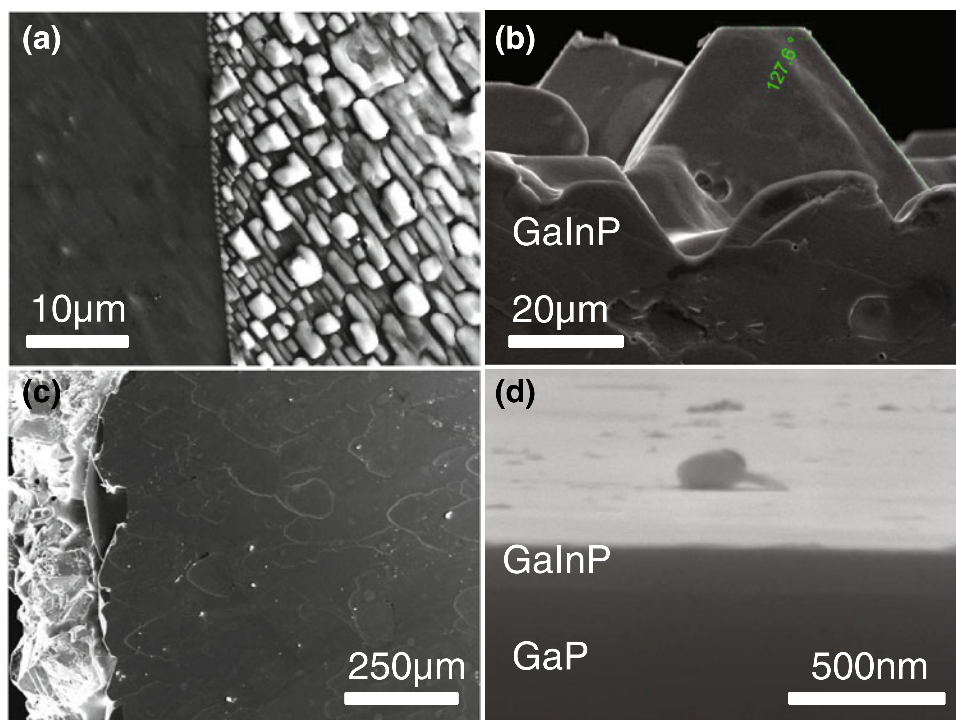

Fig. 2. (a) Plan-view SEM image of the sample grown from an In-based melt on GaP (100) which stayed in the covered position during temperature ramp-up; (b) cross-sectional SEM image of the sample grown from an In-based on GaP (100) which was positioned in an exposed spot during temperature ramp-up; (c) plan-view SEM image of the sample grown from an In-based on GaP (111B); (d) tilted cross-sectional SEM image of the sample in (c).

deterioration after the same heat treatment. The mechanism for surface stabilization of HCl is currently under investigation. However, it is possible that the strong P–H bond at the surface, formed by pre-treating the GaP substrates with HCl, inhibits P evaporation. In contrast, NH_4OH does not form P–H bonds with GaP.

After switching the initial position of the substrate to an exposed region, the problem of partial growth was solved and growth commenced over the entire surface of the substrate. Nevertheless, when using In-based melts, island growth was observed (Fig. 2b). The surface of the sample was very rough and incongruent indicating that 3D growth is preferred over planar growth. A closer look at the surface shows that the edges of many islands share the same slope, with an angle of 52.4° relative to the surface normal. This roughly correlates with the angle between the (100) and (111) planes, indicating a preference toward growth of $Ga_xIn_{1-x}P$ on the (111) plane.

Previous effort of growing lattice-mismatched epilayers on GaP substrates showed that the (111B) surface gave better surface morphology.[17] Therefore, in an effort to work around the problem of island growth and to investigate the effect of different substrate orientations on the epilayer morphology, GaP (111B) substrates were used. Figure 2c shows the plan-view SEM image of the surface of a sample grown on the (111B) surface. In this case, most of the growth occurred at the edge of the substrate, represented by the high contrast structures on the left side of the image. There was almost no growth on the top surface of the substrate. Random patterns observed on the surface were likely caused by the dissolution of the substrate because the GaP substrate can never be in equilibrium with the Ga-In-P melt. In fact, according to the etch-back and regrowth model proposed by Woodall and Hovel,[18] a very thin layer of $Ga_xIn_{1-x}P$ is expected to grow on the GaP substrate. Figure 2d confirms the model, which shows the tilted cross-sectional SEM image of the same sample in Fig. 2c. The thickness of the $Ga_xIn_{1-x}P$ layer was around 140 nm. However, this $Ga_xIn_{1-x}P$ layer was not continuous across the entire surface of the substrate.

As a consequence of the consistent island growth from In-based melts, experiments using Sn-based melts were performed. The first sample obtained from a Sn-based melt is a sample which experienced first the standard growth at a slow cooling rate, followed by a rapid cooling growth when the furnace was shut off. From the cross-sectional SEM image, two different epilayers can be observed (Fig. 3). The first one, which lies immediately on top of the GaP substrate, was grown during the slow cooling phase. According to the EDS line scan, this layer corresponds to a graded composition of $Ga_xIn_{1-x}P$. The grading in composition is a result of the depletion of Ga in the melt. The second layer, grown during the rapid cooling period, was very thick and had a composition close to pure InP. The observations from this sample suggest that not only can $Ga_xIn_{1-x}P$ layers be grown directly on GaP substrates with good surface morphology but also that the composition of $Ga_xIn_{1-x}P$ can be altered by changing the cooling rate.

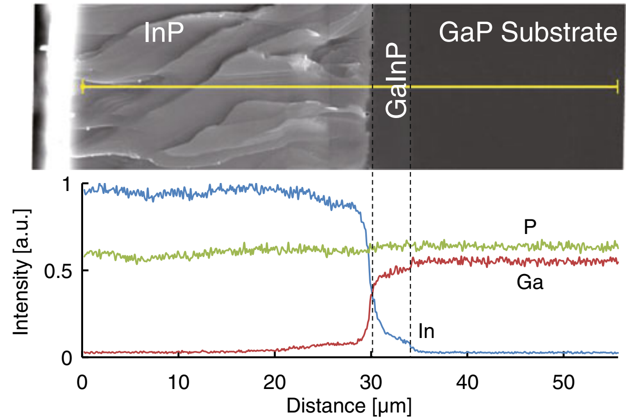

Fig. 3. Cross-sectional SEM image (*top*) with corresponding EDS line scan (*bottom*) of the sample grown from a Sn-based melt on GaP (111B) which experienced both the standard growth at a slow cooling rate, followed by a rapid cooling growth.

Two sets of experiments were then set up to further investigate the effects of growth parameters on the composition of the $Ga_xIn_{1-x}P$ epilayer. The first experiment focused on the effect of melt-back temperature. In this case, the dissolution of the GaP growth substrate was the only step that introduced Ga into the melt. Therefore, changing the amount of GaP dissolved at the beginning of the growth, by changing the melt-back temperature, should also affect the amount of Ga in the melt. Assuming equal amounts of In in the melt, different amounts of Ga would lead to different resulting compositions of $Ga_xIn_{1-x}P$.

In general, samples grown from Sn-based melts exhibited smooth and mirror-like surfaces (Fig. 4). The epilayer compositions were characterized by HRXRD (Fig. 5). Due to the depletion of Ga in the melt during the growth of a thick layer, the epilayers were graded. Therefore, two parameters were used to characterize the layer composition: minimum GaP fraction (*Min*) and maximum GaP fraction (*Max*). The *Min* and *Max* values are determined by fitting the measured curves with simulated ones using PANalytical Epitaxy software, assuming convex graded epilayers. Plotting the composition of $Ga_xIn_{1-x}P$ as a function of melt-back temperature, Fig. 6 is obtained. Both the minimum and the maximum GaP fractions increased as the melt-back temperature increased, consistent to our predictions in the last paragraph. In addition, the range of compositional grading decreased as the melt-back temperature increased, because the distribution coefficient of Ga decreases with increasing Ga concentration at high GaP fractions in the solid.[19]

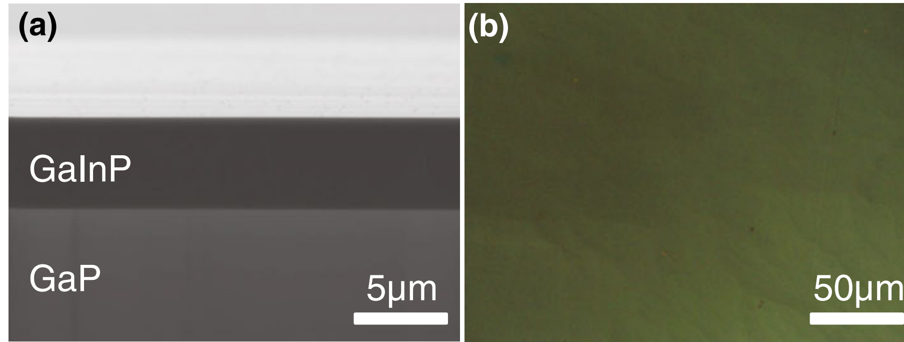

Fig. 4. (a) Tilted cross-sectional SEM image with (b) corresponding Nomarski optical micrograph of the sample grown from a Sn-based melt on GaP (100) with 5 °C of melt-back temperature.

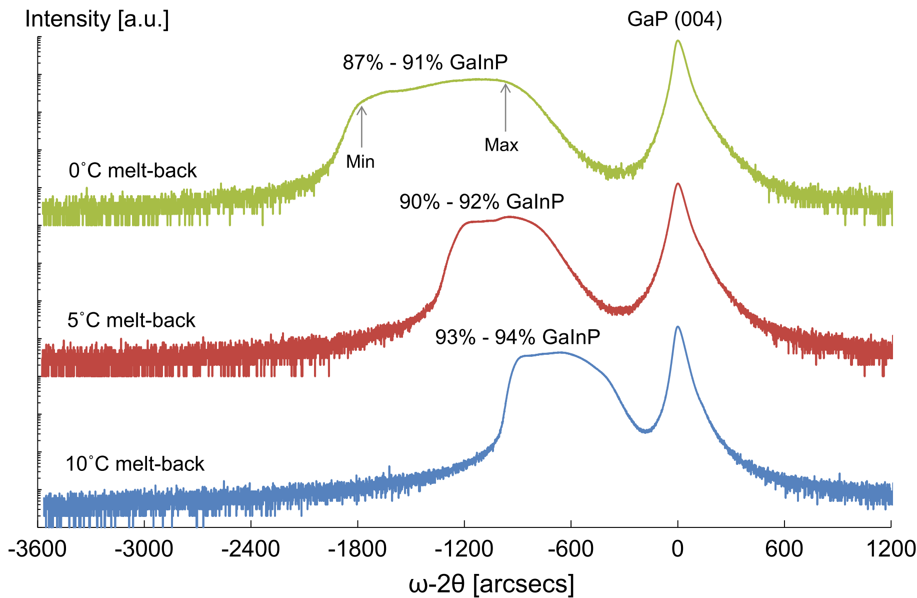

Fig. 5. XRD triple axis coupled scan of samples grown on GaP (100) using a Sn-based melt with different melt-back temperatures. The substrates were positioned under the melt at 700 °C and the growth occurred at a cooling rate of 0.33 °C/min.

PVTEM images for the sample with 5 °C of melt-back temperature were also obtained at the upper regions of the $Ga_xIn_{1-x}P$ epilayer (Fig. 7), and the TDD calculated from the PVTEM images over an area of 233.28 μm^2 is around 6×10^8 cm^{-2}.

The second set of experiments using Sn-based melts was designed to understand the effect of cooling rate. Again, the surface of these samples was generally smooth and mirror-like, similar to those shown in Fig. 4. The thicknesses of the epilayers for the sample with 0.33, 3, and 5 °C/min of cooling rate were around 9.3, 4.9, and 3.6 μm, respectively. Results from HRXRD coupled scans are shown in Fig. 8. Since most of the epilayers were heavily graded, *Min* and *Max* are used again to characterize the limits of layer composition.

Plotting the composition of $Ga_xIn_{1-x}P$ as a function of cooling rate, Fig. 9 is obtained. Maximum GaP fractions in the graded layers stayed the same, whereas minimum GaP fractions decreased with

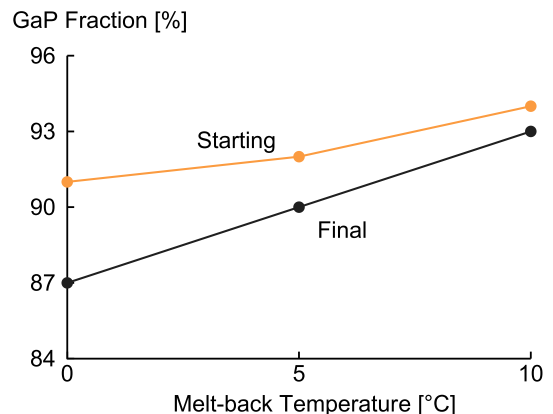

Fig. 6. Composition of $Ga_xIn_{1-x}P$ epilayers of the samples in Fig. 5 as a function of melt-back temperature. The starting and the final composition represent the maximum and the minimum GaP fraction in the graded epilayers, respectively.

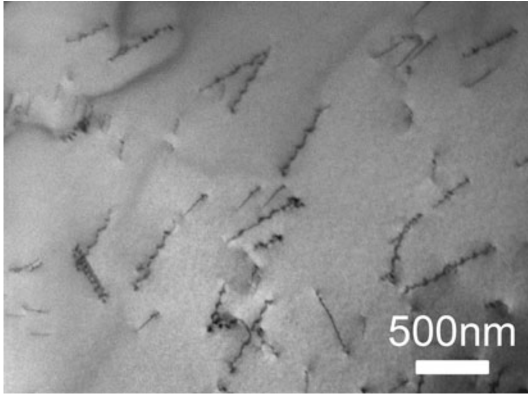

Fig. 7. PVTEM ($g = 220$) micrograph at an upper region of the $Ga_xIn_{1-x}P$ epilayer for the sample with 5 °C of melt-back temperature. The TDD over a survey area of 233.28 μm^2 is around 6×10^8 cm^{-2}.

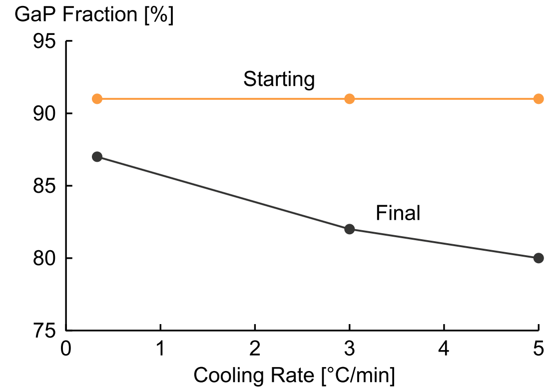

Fig. 9. Composition of $Ga_xIn_{1-x}P$ epilayers of the samples in Fig. 8 as a function of cooling rate. The starting and the final composition represent the maximum and the minimum GaP fraction in the graded epilayers, respectively.

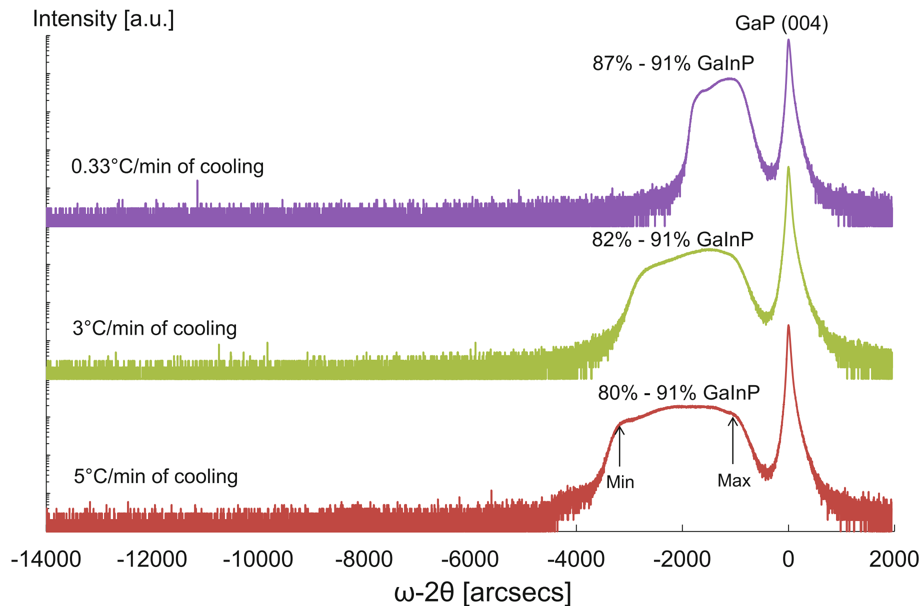

Fig. 8. XRD triple axis coupled scan of samples grown on GaP (100) using a Sn-based melt at a starting growth temperature of 700 °C with different cooling rates..

increasing cooling rate. Both trends are expected and correlates with the phenomenon previously observed in LPE of AlGaAs.[19] Because the growth of the samples all started with the same condition and the cooling rate cannot change abruptly at the beginning of growth, compositions of the initial epilayers from the three samples should be the same and equal to the maximum GaP fraction. Although the grading in the epilayer could be caused by the depletion of Ga in the melt, the decreasing thicknesses of the epilayers as the cooling rate increases indicates that the effect of Ga depletion actually diminishes as cooling rate increases. Therefore, the increasing range of compositional grading in the epilayer can only be explained by increased cooling rates. As cooling rate increases, the growth of $Ga_xIn_{1-x}P$ becomes diffusion-limited.[20] In other words, the amount of Ga incorporated into the lattice depends on the diffusion rate of Ga from the bulk of the melt to the liquid–solid growth interface. In raising the cooling rate, the crystal grows faster, but the amount of Ga available at the growth interface is limited by diffusion at the growth temperature. In incorporation tends not to be limited by diffusion because the distribution coefficient of In is much smaller than the distribution coefficient of Ga in the melt, hence its depletion will be much less significant compared to the depletion of Ga. As a result, the GaP fraction in the epilayer decreases on average.

The grading is a result of growth before a stable cooling rate is reached. Also, even when the cooling rate becomes stable, mass transport in the melt is

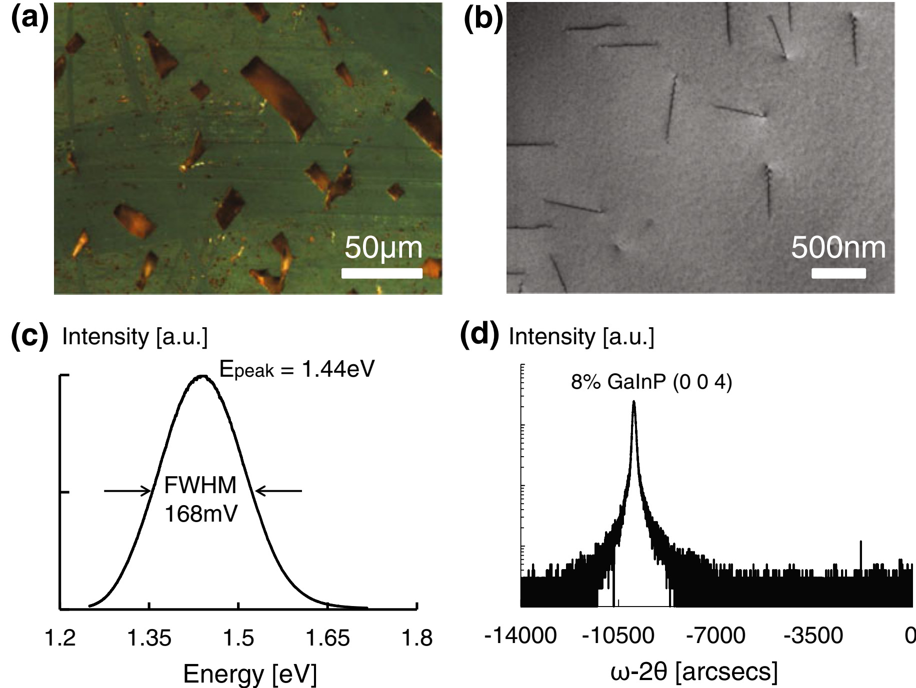

Fig. 10. (a) Nomarski optical micrograph, (b) PVTEM (g = 220) micrograph, (c) room temperature PL spectrum and (d) XRD triple-axis coupled scan of the sample grown from a Sn-based melt on GaP (100) cooled to room temperature from 700 °C at a large cooling rate. The TDD determined from PVTEM over a survey area of 207.36 μm^2 is around 2×10^8 cm^{-2}. The XRD scan is referenced to GaP (004) at 0 arcsecs.

still likely to evolve. Nevertheless, if the growth occurred at steady-state with respect to the melt concentration gradient, then the layer composition should be almost constant. To verify this, an additional sample was fabricated, which was cooled to room temperature at a rate of 9 °C/min during the growth. Cooling the system to room temperature allows sufficient time for the growth to happen at steady state with respect to the melt concentration gradient. Since we did not use any artificial cooling techniques, the cooling rate of 9 °C/min was only consistently observed when the apparatus temperature was above 600 °C. After that, the cooling rate dropped as the temperature decreased. This sample exhibited pits on its surface, as shown in Fig. 10a. We believe these formed to relax the strain caused by the huge lattice mismatch of around 7.2 % for the given composition of GaInP. A sharp peak was observed in its HRXRD-coupled scan (Fig. 10d), indicating a thick In-rich GaInP epilayer without compositional grading. The peak corresponds to a composition of $Ga_{0.08}In_{0.92}P$. Room temperature PL was observed for this sample (Fig. 10c). The spectrum indicates a bandgap energy of E_g = 1.44 eV from the epilayer, which corresponds to a composition of $Ga_{0.11}In_{0.89}P$. This closely correlates to the composition as determined by XRD. The FWHM of the PL spectrum is 168 meV. Finally, PVTEM analysis (Fig. 10b) performed on the upper regions of this sample revealed a TDD of around 2×10^8 cm^{-2} over a survey area of 207.36 μm^2. This measured TDD is around 30 times larger than that reported for $Ga_{0.74}In_{0.26}P$ grown on GaP by MBE,[21] mainly because of the absence of a metamorphic buffer layer.

CONCLUSION

In this work, layered growth of $Ga_xIn_{1-x}P$ on GaP substrates at large lattice mismatch was achieved by single-step LPE using a Sn-based melt. The composition of the epilayer was affected by both the cooling rate and the melt-back temperature at the beginning of growth. At large cooling rates, heavily graded epilayers were observed mainly due to growth before steady-state with respect to the melt concentration gradient was reached. Therefore, obtaining an epilayer with constant desired composition by the method of altering the cooling rate requires the growth to happen at steady state, which is under further investigation.

ACKNOWLEDGEMENT

We thank TEM Analysis Services for the PVTEM micrographs and Stephanie Tomasulo and Minjoo Larry Lee for useful discussion in determining TDD.

REFERENCES

1. T. Gessmann and E.F. Schubert, *J. Appl. Phys.* 95, 2203 (2004).
2. E.F. Schubert, *Light-Emitting Diodes* (Cambridge: Cambridge University Press, 2003), pp. 1–7.
3. M.R. Krames, O.B. Shchekin, R. Mueller-Mach, G.O. Mueller, L. Zhou, G. Harbers, and M.G. Craford, *J. Disp. Technol.* 3, 160 (2007).

4. T. Suzuki, A. Gomyo, and S. Iijima, *J. Cryst. Growth* 93, 396 (1988).
5. T. Suzuku, *Spontaneous Ordering in Semiconductor Alloys*, ed. A. Mascarenhas (New York: Kluwer, 2002), pp. 1–43.
6. J. Nishizawa and S. Yoshida, *J. Cryst. Growth* 78, 274 (1986).
7. S. Nakayama, M. Kaneko, S. Aizawa, K. Kashiwa, and N.S. Takahashi, *J. Cryst. Growth* 236, 132 (2002).
8. S. Uematsu, M. Nomoto, S. Nakayama, and N.S. Takahashi, *Cryst. Res. Technol.* 40, 1113 (2005).
9. J.M. Woodall and H.J. Hovel, *J. Cryst. Growth* 39, 108 (1977).
10. K.H. Montgomery, Novel Approaches for Wide Band GaP Solar Cells, PhD dissertation, Purdue University, West Lafayette (2012).
11. T. Berdinskikh, H.E. Ruda, X.Y. Mei, and M. Buchanan, *J. Electron. Mater.* 27, 114 (1998).
12. T. Sugiura, A. Tanaka, and T. Sukegawa, *J. Cryst. Growth* 46, 595 (1979).
13. W. Korber and K.W. Benz, *J. Cryst. Growth* 73, 179 (1985).
14. J.L. Shay and K.J. Bachmann, *Appl. Phys. Lett.* 24, 192 (1974).
15. A. Onton, M.R. Lorenz, and W. Reuter, *J. Appl. Phys.* 42, 3420 (1971).
16. I. Vurgaftman, J.R. Meyer, and L.R. Ram-Mohan, *J. Appl. Phys.* 89, 5815 (2001).
17. J.M. Woodall, R.M. Potemski, and S.E. Blum, *Appl. Phys. Lett.* 20, 375 (1972).
18. J.M. Woodall and H.J. Hovel, *Appl. Phys. Lett.* 30, 492 (1977).
19. J.M. Woodall, H. Rupprecht, and W. Reuter, *J. Electrochem. Soc.* 116, 899 (1969).
20. E. Kuphal, *Appl. Phys. A* 52, 380 (1991).
21. S. Tomasulo, J. Faucher, J.R. Lang, K.N. Yaung, and M.L. Lee, Proceedings of 39th IEEE Photovoltaic Specialists Conference, Tampa, FL (2013).